



HAL
open science

Prompt and delayed γ spectroscopy of neutron-rich ^{94}Kr and observation of a new isomer

R.-B. Gerst, A. Blazhev, N. Warr, J. Wilson, M. Lebois, N. Jovančević, D. Thisse, R. Canavan, M. Rudigier, D. Etasse, et al.

► To cite this version:

R.-B. Gerst, A. Blazhev, N. Warr, J. Wilson, M. Lebois, et al.. Prompt and delayed γ spectroscopy of neutron-rich ^{94}Kr and observation of a new isomer. *Physical Review C*, 2020, 102 (6), pp.064323. 10.1103/PhysRevC.102.064323 . hal-03094623

HAL Id: hal-03094623

<https://hal.science/hal-03094623v1>

Submitted on 4 Jan 2021

HAL is a multi-disciplinary open access archive for the deposit and dissemination of scientific research documents, whether they are published or not. The documents may come from teaching and research institutions in France or abroad, or from public or private research centers.

L'archive ouverte pluridisciplinaire **HAL**, est destinée au dépôt et à la diffusion de documents scientifiques de niveau recherche, publiés ou non, émanant des établissements d'enseignement et de recherche français ou étrangers, des laboratoires publics ou privés.

Prompt and delayed γ -spectroscopy of the neutron-rich ^{94}Kr and observation of a new isomer

R.-B. Gerst,^{1,a} A. Blazhev,¹ N. Warr,¹ J. N. Wilson,² M. Lebois,² N. Jovančević,² D. Thisse,² R. Canavan,³ M. Rudigier,^{3,4} D. Étasse,⁵ E. Adamska,⁶ P. Adsley,² A. Algora,⁷ M. Babo,² K. Belvedere,³ J. Benito,⁸ G. Benzoni,⁹ A. Boso,¹⁰ S. Bottoni,^{11,9} M. Bunce,¹⁰ R. Chakma,² N. Cieplicka-Oryńczak,¹² S. Courtin,^{13,14} M. L. Cortés,¹⁵ P. Davies,¹⁶ C. Delafosse,² M. Fallot,¹⁷ B. Fornal,¹² L. Frail,⁸ D. Gjestvang,¹⁸ A. Gottardo,¹⁹ V. Guadilla,¹⁷ G. Häfner,^{1,2} K. Hauschild,² M. Heine,¹³ C. Henrich,⁴ I. Homm,⁴ F. Ibrahim,² Ł. W. Iskra,^{9,12} P. Ivanov,¹⁰ S. Jazwari,^{3,10} A. Korgul,⁶ P. Koseoglou,^{4,20} T. Kröll,⁴ T. Kurtukian-Nieto,²¹ L. Le Meur,¹⁷ S. Leoni,^{11,9} J. Ljungvall,² A. Lopez-Martens,² R. Lozeva,² I. Matea,² K. Miernik,⁶ J. Nemer,² S. Oberstedt,²² W. Paulsen,¹⁸ M. Piersa,⁶ Y. Popovitch,² C. Porzio,^{11,9,23} L. Qi,² D. Ralet,²⁴ P. Regan,^{3,10} D. Reygadas-Tello,²⁵ K. Rezykina,²⁶ V. Sánchez-Tembleque,⁸ C. Schmitt,¹³ P.-A. Söderström,⁴ C. Sürder,⁴ G. Tocabens,² V. Vedia,⁸ D. Verney,² B. Wasilewska,¹² J. Wiederhold,⁴ M. Yavachova,²⁷ F. Zeiser,¹⁸ and S. Ziliani^{11,9}

¹*Institut für Kernphysik, Universität zu Köln, 50937 Köln, Germany*

²*Université Paris-Saclay, CNRS/IN2P3, IJCLab, 91405 Orsay, France*

³*Department of Physics, University of Surrey, Guildford GU2 7XH, United Kingdom*

⁴*Technische Universität Darmstadt, Fachbereich Physik, Institut für Kernphysik, 64289 Darmstadt, Germany*

⁵*LPC Caen, 6 Boulevard Maréchal Juin, 14000 Caen, France*

⁶*Faculty of Physics, University of Warsaw, PL 02-093 Warsaw, Poland*

⁷*IFIC, CSIC-University of Valencia, Valencia, Spain*

⁸*Grupo de Fisica Nuclear & IPARCOS, Universidad Complutense de Madrid, CEI Moncloa, 28040 Madrid, Spain*

⁹*INFN sez. Milano, Via Celoria 16, 20133 Milano, Italy*

¹⁰*National Physical Laboratory, Hampton Road, Teddington, Middlesex TW11 0LW, United Kingdom*

¹¹*Dipartimento di Fisica, Università degli Studi di Milano, Via Celoria 16, 20133 Milano, Italy*

¹²*Institute of Nuclear Physics, Polish Academy of Sciences, PL-31342 Krakow, Poland*

¹³*IPHC, 23 rue du Loess, 67037 Strasbourg, France*

¹⁴*CNRS, UMR7178, 67037 Strasbourg, France*

¹⁵*RIKEN Nishina Center, 2-1 Hirosawa, Wako, Saitama 351-0198, Japan*

¹⁶*School of Physics and Astronomy, University of Manchester, Oxford Road, Manchester M13 9PL, United Kingdom*

¹⁷*Subatech, IMT-Atlantique, Université de Nantes, CNRS-IN2P3, F-44307 Nantes, France*

¹⁸*University of Oslo, Department of Physics, P.O. Box 1048, Blindern, 0316 Oslo, Norway*

¹⁹*INFN Laboratori Nazionali di Legnaro, Viale dell'Università, 2, I-35020 Legnaro, Italy*

²⁰*GSI Helmholtzzentrum für Schwerionenforschung GmbH, Planckstr. 1, 64291 Darmstadt, Germany*

²¹*CENBG, UMR5797, Université de Bordeaux, CNRS, F-33170 Gradignan, France*

²²*European Commission, Joint Research Centre, Directorate G for Nuclear Safety and Security, Unit G.2, 2440 Geel, Belgium*

²³*TRIUMF, 4004 Wesbrook Mall, Vancouver, BC V6T 2A3, Canada*

²⁴*Grand Accélérateur National d'Ions Lourds, Bd Henri Becquerel, 14076 Caen, France*

²⁵*School of Computing, Engineering and Mathematics,*

University of Brighton, Brighton, BN2 4GJ, United Kingdom

²⁶*Institute for Nuclear and Radiation Physics, KU Leuven, 3000 Leuven, Belgium*

²⁷*Institute for Nuclear Research and Nuclear Energy,*

Bulgarian Academy of Sciences, 1784 Sofia, Bulgaria

Prompt and delayed γ -ray spectroscopy of the neutron-rich ^{94}Kr was performed, as part of the fission campaign at the ALTO facility of the IPN Orsay, using the fast-neutron induced fission reaction $^{238}\text{U}(n,f)$ in combination with the ν -Ball array, a novel hybrid γ -spectrometer for energy and lifetime measurements. Several new yrast and non-yrast transitions were observed for the first time, extending the previously known level scheme. Additionally, we report on the observation of a new short-lived isomer at 3444 keV with a half-life of 32(3) ns. The analysis of the Nilsson orbitals obtained from Gogny Cranked Hartree-Fock-Bogoliubov (CHFB) calculations suggests a (9^-) spin and an oblate deformation for this isomer corresponding to a two-quasineutron state indicating a very similar isomeric structure as the neighboring isotones ^{96}Sr and ^{92}Se .

I. INTRODUCTION

The study of nuclear properties far away from the valley of stability to investigate their dependence on the number of neutrons and protons is crucial to our understanding of the atomic

nucleus and the nuclear forces. One important feature is the evolution of nuclear shape along the isotopic chains, which is determined by the interplay between the macroscopic and microscopic properties. In some mass regions, this interaction between collective and single-particle degrees of freedom can lead to a very sudden growth of collectivity. One way of interpreting this drastic behavior is within the context of the coexistence of two distinct configurations at low excitation energies, one spherical and one deformed, where the latter

^a Corresponding author: rgerst@ikp.uni-koeln.de

suddenly becomes energetically more favorable [1]. Experimentally, this usually manifests itself in even-even nuclei in a sudden drop of the $E(2_1^+)$ energy and the gradual lowering of an excited 0^+ state [2, 3], which constitutes the bandhead of the competing configuration. The region of $A \sim 100$ exhibits one of the most abrupt shape transitions of this type. Experimentally, it was established that the isotopic chains of Sr, Zr, and Mo exhibit a very sudden onset of deformation going from $N = 58$ to $N = 60$ [4–9]. Mass measurements of krypton $Z = 36$ and rubidium $Z = 37$ isotopes were performed [10], labeling $Z = 37$ as the boundary of this region of deformation. Additionally, recent γ -spectroscopy identified ^{97}Rb as the lower corner stone of this phenomenon [11]. In agreement with this, earlier experimental results had established a rather gradual development of collectivity in krypton isotopes with a slow decrease in $E(2_1^+)$ up to $N = 60$ [12, 13] and no evidence for low-lying intruder states. However, more recent studies revealed a slightly different behavior for $N \geq 60$ [14, 15]. In ^{96}Kr , an unexpectedly low value of the ratio $E(4_1^+)/E(2_1^+)$ was determined experimentally [14]. In $^{98,100}\text{Kr}$, a significant drop of $E(2_1^+)$ was observed and for ^{98}Kr a low-lying ($0_2^+, 2_2^+$) state was identified [15]. The discovery of a low-lying ($0_2^+, 2_2^+$) state in ^{98}Kr , as evidence for a coexisting deformed configuration, also encourages the search for excited bands in the Kr isotopes with $N < 60$ to further investigate the presence of deformed coexisting configurations in this region. To examine this development of shape coexistence in Kr isotopes, different theoretical approaches have been used [13, 16]. Most recently, Gogny-D1M calculations were performed by Nomura *et al.* [17] for the even krypton isotopes. For $^{88-92}\text{Kr}$, this reveals a defined γ -softness that develops into a γ -soft oblate minimum for ^{94}Kr . For the isotopes with $N > 58$, the energy surfaces show a pronounced prolate-oblate shape coexistence further cementing the experimental results. Hence, the changes between ^{94}Kr and ^{96}Kr are crucial for the understanding of the shape evolution in the krypton isotopes specifically and in this region generally.

In this paper, we report on the observation of a new $32(3)$ ns isomer at 3444 keV in ^{94}Kr together with several new yrast and non-yrast γ -transitions extending the previously known level scheme. Prior to this work, the only published γ -transitions in ^{94}Kr were 665.5 keV, 853.2 keV, and 1001.3 keV, measured via Coulomb excitation at the REX-ISOLDE facility by Albers *et al.* [12] and following spontaneous fission of ^{248}Cm with the EUROGAM 2 array by Rząca-Urban *et al.* [18]. On the basis of angular correlation analysis, a spin and parity of 2^+ and of 4^+ were assigned to the levels at 665.5 keV and 1518.7 keV, respectively, with the remaining transition of 1001.3 keV populating the 4^+ level [18].

II. EXPERIMENT

The measurement, presented in this paper, was performed in 2018 as part of the ν -Ball campaign at the ALTO facility at the IPN Orsay in France, using the $^{238}\text{U}(n,f)$ fast-neutron induced fission reaction [19, 20]. Here, ^{94}Kr was populated much more strongly with a yield of 0.8 % as opposed to

0.04 % for fission of ^{248}Cm [21]. The directional fast-neutron beam was produced with the neutron source LICORNE [22], which uses the $p(^7\text{Li}, ^7\text{Be})n$ reaction in inverse kinematics. The ^7Li beam was provided by the 15 MV Tandem Van de Graaff accelerator in a pulsed mode with a 2 ns pulse width and a repetition period of 400 ns. The ^7Li beam entered the hydrogen gas cell of LICORNE through a 2.8 μm tantalum foil. During the experiment a 16 MeV ^7Li beam was used together with a 3.5 cm H_2 gas cell with a pressure of 1.2 atm to maximize the neutron flux. The neutrons then impinged on an 81 g ^{238}U sample with a composition of 99.8 % ^{238}U and 0.2 % ^{235}U produced by JRC-Karlsruhe. The fissile material was arranged in five thin disks over a distance of 8 cm to allow low-energy γ -rays to escape from the target. No Doppler correction was required as the fission fragments were stopped in the material. Therefore, the energy resolution of the detectors only depended on their intrinsic resolution giving the spectrometer an excellent resolving power. The ^{238}U sample was placed at a distance of 4 cm to LICORNE to maximize the fission rate. ^{238}U has a fission threshold of ~ 1.2 MeV and in comparison to ^{235}U a very small fission cross section of 0.5 barn at this energy [23]. During the experiment an average primary ^7Li beam flux of $2 \cdot 10^{10}/\text{s}$ was achieved, which translated into a secondary neutron beam of $2 \cdot 10^6/\text{s}$ and a rate of 10^4 fission events/s. Additionally, a neutron detector was placed behind the setup to measure the neutron energy (~ 1.7 MeV) via time-of-flight, but was not relevant to this analysis. The ^{238}U sample was

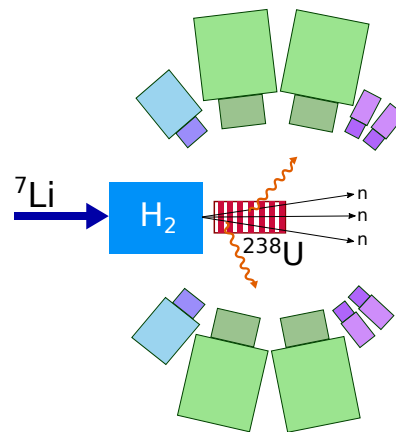


Figure 1. Schematic drawing of the ν -Ball array, coupled to the LICORNE fast-neutron source. The $p(^7\text{Li}, ^7\text{Be})n$ reaction produced a focused fast-neutron beam which induced fission in the ^{238}U material. The γ -rays stemming from the excited fission products were measured with ν -Ball, consisting of 10 Phase I HPGe (blue), 24 Clover HPGe (green), and 20 LaBr_3 (violet) detectors. The solid angle coverage was approximately 70%.

situated at the center of the ν -Ball array, a novel hybrid High Purity Germanium (HPGe)- LaBr_3 γ -spectrometer that was designed to combine the excellent energy and timing resolution of the two detector types, respectively [20]. A schematic view of the LICORNE chamber and the detector setup can be seen in Fig. 1. During the fission campaign, the array consisted of 24 HPGe Clover detectors, 10 coaxial

Phase I HPGe detectors, all with BGO Compton shielding, and 20 LaBr₃ detectors without Compton shielding. The Phase I detectors were placed in a ring at a backward angle of 133.5°, and the Clover detectors were placed in two rings around 90°. The LaBr₃ detectors were mounted in two rings around 40°. Because of the presence of the directional neutron beam, no γ -detector was placed at extreme forward angles ($< 20^\circ$) in order to avoid neutron-induced damages to the detectors. Calibration measurements were performed using ¹⁵²Eu and ⁶⁰Co standard γ -sources. The combined resolution of all HPGe channels was 2.35 keV at 1 MeV, with resolutions of single detectors ranging from 1.7 keV for Clover detectors to 2.9 keV for Phase I detectors. A photopeak efficiency of 6.7 % at 1.3 MeV for the HPGe detectors was simulated with GEANT4 before the campaign [20]. The measured values were in excellent agreement for energies above 344 keV. For lower energies the efficiency was slightly lower than expected due to absorption in the aluminum gas cell of LICORNE [20]. The measurement was performed in a triggerless mode and the FASTER data acquisition system was used for processing [24]. In total, approximately 216 hours of data were taken. In the following, only results from the analysis of the HPGe detectors will be presented.

III. DATA ANALYSIS AND RESULTS

The 400 ns pulsed beam makes it possible to investigate prompt and delayed γ -transitions separately and in coincidence. For the HPGe detectors, the prompt peak in the timing distribution has a FWHM of ~ 23 ns, which includes the intrinsic time resolution of the detectors, the beam pulse width, and the time-of-flight differences of the neutrons over the target length. For γ -rays emitted outside of the prompt time region, the energy spectra can be cleaned significantly by setting a timing condition of $T \geq 35$ ns after the beam pulse, with the higher limit set dependent on the half-life range being investigated. A timing gate of $T \leq 35$ ns after beam pulse was used to specifically look for prompt γ -rays. Additionally, the background could be reduced significantly by optimizing multiplicity conditions for the number of detected γ -rays in the full and in the delayed time windows. In this case, events were built with the total γ -multiplicity of ≥ 5 and ≤ 17 with a minimum of two HPGe detectors fired to select fission and to suppress low-multiplicity events such as inelastic scattering. An additional constraint on the delayed multiplicity was used after the number of delayed transitions was determined.

The prompt background-subtracted energy spectrum produced by a gate on the 4_1^+ to 2_1^+ 853.8 keV transition is presented in the upper panel of Fig. 2. The previously published transitions, 665.5 keV and 1001.3 keV, are the strongest peaks in the spectrum along with several lines from the fission partner isotopes ^{142–144}Ba. Three additional lines at 834.9 keV, 852.9 keV and 1267.1 keV are present. With an additional gate on the 1001.8 keV transition (Fig. 2 lower panel), the peak at 1267.1 keV disappears which suggests a parallel branch. This will be explored further in the analysis

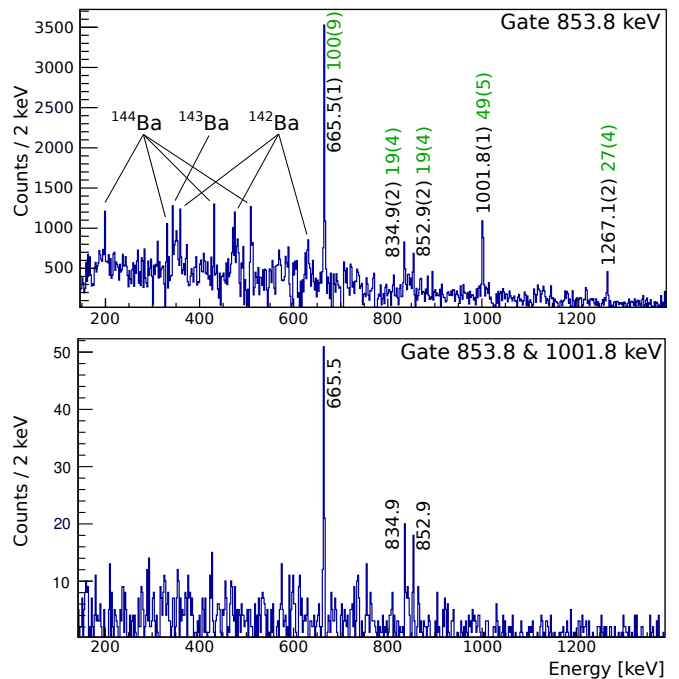


Figure 2. Upper panel: Background-subtracted energy spectrum coincident to the gate on the 853.8 keV 4_1^+ to 2_1^+ transition in the prompt time window. The efficiency-corrected intensities normalized to the strongest transition at 665.5 keV (green) are shown next to the peaks. Only events where at least three different HPGe detector hits were recorded are considered. Lower panel: The energy spectrum after a second gate on 1001.8 keV is applied.

of the delayed time window. The other two peaks remain visible, as can be seen in the lower panel of Fig. 2, which proves them to be in coincidence with the 1001.8 keV and 4_1^+ to 2_1^+ transitions. The peak at 852.9 keV is very close in energy to the 4_1^+ to 2_1^+ transition of 853.8 keV. But since this transition is visible when gating on the 4_1^+ to 2_1^+ transition in any double gate combination of yrast states, it is assumed that such a transition at 852.9 keV exists. Due to their coincidence relation to the previously established yrast states, we place the 834.9 keV and 852.9 keV transitions above the three previously known transitions, see Fig. 5. The ordering and tentative spin assignment as (8^+) and (10^+) will be clarified by the analysis of delayed γ -transitions in the subsequent discussion. Additionally, three transitions, 665.5 keV, 551.2 keV, and 695.3 keV, were observed in coincidence with each other. Even though 665.5 keV matches the known 2_1^+ to 0_1^+ transition energy, for fission data a second gate on a known transition would normally be necessary to reliably assign these transitions to ⁹⁴Kr. However, in ⁹⁴Kr a transition of approximately 550 keV was observed in coincidence with the 665.5 keV transition [25] in the data taken during the 2015 SEASTAR campaign at RIKEN [26]. Therefore, the transitions 551.2 keV and 695.3 keV are placed in the level scheme as seen in Fig. 5. They are not seen in coincidence with any other prompt or delayed transition.

For the analysis of the delayed γ -rays, besides the total multiplicity of ≥ 5 and ≤ 17 , the additional constraint on

the delayed multiplicity was set, respective to the expected number of delayed transitions in the different isotopes. In Fig. 3, the background-subtracted energy spectrum gated on the 4_1^+ to 2_1^+ in a time window of 35 - 180 ns after beam pulse with a delayed multiplicity of ≥ 2 and ≤ 6 can be seen. The delayed time window was optimized after the half-life of the new isomer had been determined. Next to three coincident peaks at 665.6 keV, 1001.8 keV and 1267.1 keV previously visible in the gated prompt spectrum, three additional peaks at 186.8 keV, 470.7 keV, and 736.0 keV show up.

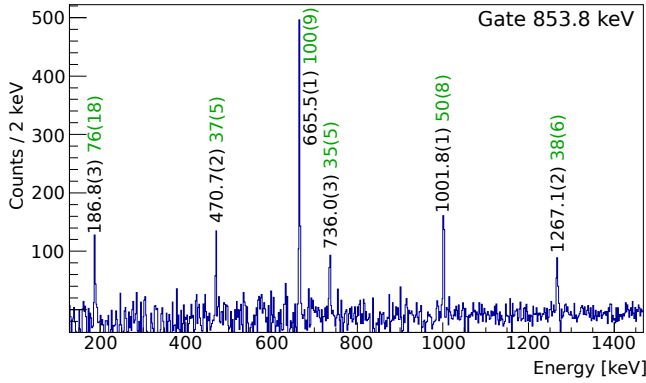


Figure 3. Background-subtracted energy spectrum coincident with the gate on the 4_1^+ to 2_1^+ 853.8 keV transition in the delayed 35-180 ns time window. The efficiency-corrected intensities normalized to the strongest transition at 665.5 keV (green) are shown next to the peaks.

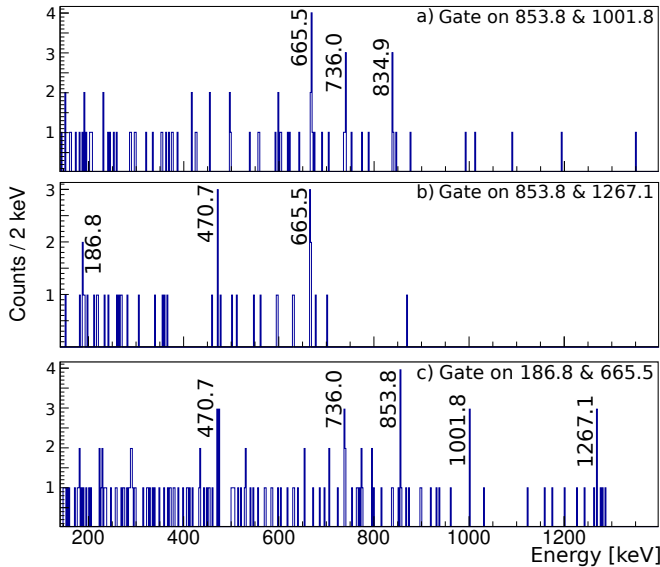


Figure 4. Double gated energy spectra in the delayed 35 - 180 ns time window. a) Gated on the 853.8 keV and 1001.8 keV transitions. b) Gated on the 853.8 keV and 1267.1 keV transitions. c) Gated on the 186.8 keV and 665.5 keV transitions.

By looking at different delayed double-gates, one can observe two parallel decay paths on top of the 4_1^+ to 2_1^+ transition. When comparing the spectra generated by gating on the 4_1^+ to 2_1^+ and the 1001.8 keV transition and the 4_1^+ to 2_1^+

and 1267.1 keV transition, as seen in Figs. 4 a) and b) respectively, only the 2_1^+ to 0_1^+ 665.5 keV transition remains as coincident to both double gates. If we look at the efficiency-corrected intensities, we find that $I_{853.8} \approx I_{1001.8} + I_{1267.1}$ and $I_{186.8} \approx I_{470.7} + I_{736.0}$. When double gating on the 186.8 keV and 2_1^+ to 0_1^+ transitions, with the exception of 834.9 keV all other delayed transitions appear in coincidence (see Fig. 4 c). With this information, the level scheme was expanded as shown in Fig. 5. Concerning the 834.9 keV line, visible both in the prompt energy spectra and the double gated delayed spectrum Fig. 4 a), we assume that a non-observed 88 keV transition connects the isomeric 3444 keV level with the (8^+) level at 3356 keV. With our setup, a transition of this energy is very unlikely to be observed due to the low efficiency at that energy. The high Z and thickness of the target material attenuates low energy γ -rays strongly.

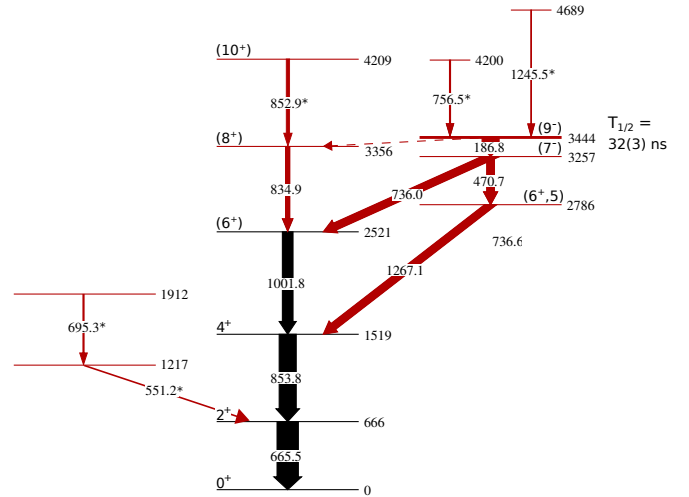


Figure 5. Level scheme constructed for ^{94}Kr . Energies are given in keV. The widths of the transitions arrows correspond to their efficiency-corrected intensities. New transitions and levels are shown in red. Transitions denoted by asterisk are only observed in the prompt time window.

To determine the half-life of the 3444 keV isomer, the data were sorted into a $\gamma\gamma$ T-cube to obtain the timing distribution of the intensities of the delayed coincidences of ^{94}Kr . As test cases, the isotopes ^{134}Te and ^{95}Sr with well-known isomers with half-lives of 164.1(9) ns and 21.9(5) ns [27, 28], respectively, were used for every step to verify the analysis method. For these cases, we obtain half-lives of 166(6) ns and 21.0(5) ns, in excellent agreement with the literature values. In Fig. 6, the time distribution used for the determination of the isomer half-life is shown. The timing spectra for the 665.5/853.8 keV, 665.5/1001.8 keV, 665.5/470.7 keV, 853.8/470.7 keV, and 853.8/1001.8 keV prompt coincidences of transitions, which are situated below the 3444 keV isomer, were added up to maximize statistics. The other combinations of transitions below the isomer were not used here due to low statistics. The second, smaller peak in the time distribution at 75 ns is a result of the artificial boundary introduced by

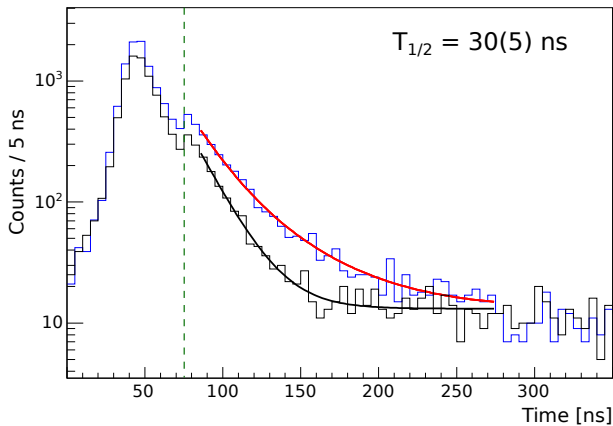


Figure 6. Time spectrum and fitted decay curve used to determine half-life of the 3444 keV isomer. For this spectrum, only events that have a delayed multiplicity of ≥ 2 and ≤ 6 in the delayed time region (beyond the dashed line) were considered. The decay curve is fitted with an exponential decay function (red) together with a time dependent background (black). To maximize statistics the time distributions of different γ -ray coincidences below the isomer were added up to one decay curve (blue).

defining and limiting the delayed multiplicity. The half-life was obtained by simultaneously fitting the time-dependent summed background spectrum of the coincidences (see black histogram in Fig. 6) together with the non-subtracted time spectrum of the five coincidence pairs (see blue histogram in Fig. 6) using the maximum likelihood method in the same manner as in Ref. [29]. By varying the energy ranges of the background, the systematic uncertainty could be estimated. Together, this yields a half-life of 30(5) ns.

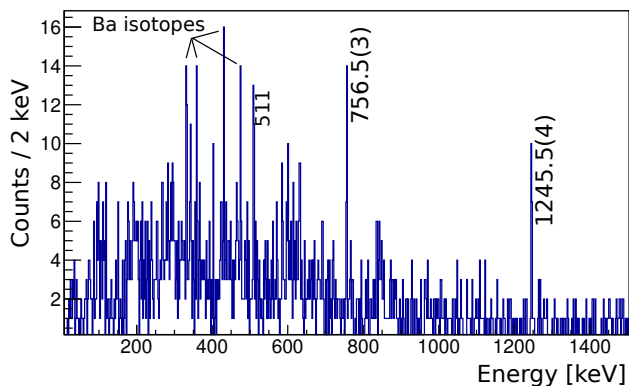


Figure 7. Background-subtracted prompt energy spectrum generated by double gating on coincidences of delayed γ -transitions below the 3444 keV isomer in the 35 - 180 ns time window.

Figure 7 shows the background-subtracted energy spectrum in the prompt time window produced by double gating on the delayed transition pairs 665.5/853.8 keV, 665.5/1001.8 keV, 665.5/1267.1 keV, 665.5/470.7 keV, 853.8/470.7 keV, 853.8/1001.8 keV and 853.8/1267.1 keV below the 3444 keV isomer in the delayed time window 35 - 180 ns, and adding

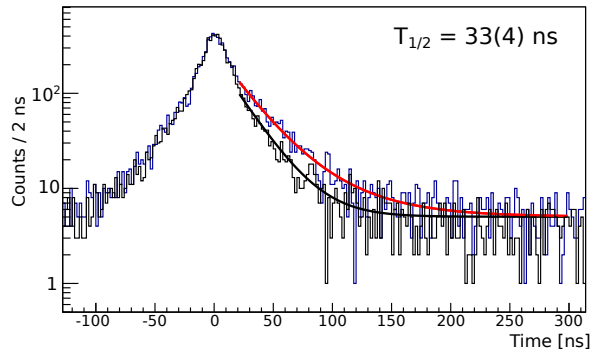


Figure 8. Prompt-delayed ΔT spectrum of prompt transitions populating and delayed transitions depopulating the 3444 keV isomer. The decay curve is fitted with an exponential decay function (red) together with a time dependent background (black). To gain statistics, several prompt-delayed transition combinations were added up to one decay curve (blue).

up the coincident prompt spectra. The strongest peaks in the resulting spectrum are the lowest transitions in the partner fission isotopes $^{142-144}\text{Ba}$ (as also seen in Fig. 2), 511 keV and two new transitions at 756.6 keV and 1245.5 keV. Accordingly, these two transitions can be placed on top of the isomer in the level scheme. Since they are not seen in coincidence to each other, we place them in parallel to each other, as seen in Fig. 5. Since these new transitions are feeding the isomeric state, the time difference between them and the delayed transitions depopulating the isomer can be used for a second determination of the isomeric half-life. In Fig. 8, the prompt-delayed $\gamma\gamma\Delta T$ -spectrum for the isomer is shown. To maximize statistics, the time differences between both prompt transitions, 756.6 keV and 1245.5 keV, feeding the isomer, and the transitions 665.5 keV, 853.8 keV, 1001.8 keV and 1267.1 keV, below the isomer, were added up. As above, the half-life was obtained by simultaneous fitting of the time-dependent summed background spectrum and the non-subtracted ΔT -spectrum of the prompt-delayed pairs. This yields a half-life of 33(4) ns in accordance with the half-life obtained from Fig. 6. Due to the independence of the two results, we can take the weighted average which results in $T_{1/2} = 32(3)$ ns. The measurement of this short-lived isomer demonstrates the capabilities of ν -Ball in this half-life range, complementary to in-flight facilities where this time range is not always accessible.

IV. DISCUSSION

The new level scheme of ^{94}Kr is shown in Fig. 5. The excitation energies are indicated next to each level. The widths of the arrows are proportional to the efficiency-corrected intensities obtained for the transitions. The two new transitions 834.9 keV and 852.9 keV, observed in the prompt time window (see Fig. 2) to be coincident with the previously published

yrast transitions [18], were assigned to be a feeding the (6_1^+) and (8_1^+) states. The ordering was deduced from the prompt coincidence analysis (see Fig. 2) and the delayed coincidence analysis (see Fig 4). The 834.9 keV transition is also observed in the delayed time window and therefore has to be below the isomeric state at 3444 keV. The state at 4209 keV, depopulated by the 852.9 keV transition in the prompt time window, needs to have a spin of $J_{4209} > 8$, with the most likely candidate being (10_1^+). The level at 2786 keV decays to the 4_1^+ level at 1519 keV, while a transition to the 6_1^+ at 2521 keV was not observed. Thus, the most probable spin-parity assignments, producing the lowest possible multipole radiation, for the 2786 keV state are ($5,6^+$). The higher level at 3257 keV, right below the isomeric state, decays to the 6_1^+ at 2521 keV and to the ($5,6^+$) level at 2786 keV, not to the 4_1^+ or 2_1^+ , which suggests a spin $J_{3257} > 6$. On top of the level, there is the 186.8 keV transition which also depopulates the isomer. Calculating the reduced transition strength based on a single-branch with the Transnuclear code [30], a transition multipolarity ≥ 3 can be excluded. For a single branch E2 transition with this energy, this yields 2.8(3) W.u. while for E1, M1, M2 the results are either much too low or much too high to be reasonably compatible with physical expectations. The most likely E2 character of this transition suggests $9^{+/-}$ and $7^{+/-}$ states as the most probable assignments for the 3444 keV isomer and the 3257 keV state, respectively. In fact, in the neighboring isotope ^{96}Sr , there is a well known 40 ns isomeric 9^- state depopulated via E2 and E1 transitions [32, 33]. This has been well described by shell-model calculations suggesting a dominant neutron $(g_{7/2}, h_{11/2})_{9^-}$ configuration [33]. This resembles the situation observed in our ^{94}Kr level scheme supporting the tentative spin assignments of (9^-), (7^-), and (8^+) for the corresponding states. Additionally in ^{96}Sr , there is a prompt cascade $10^+ \rightarrow 8^+ \rightarrow 6^+$ bypassing the isomer [32, 34] in further support of our tentative spin assignment for the 4209 keV state to be a (10^+). Furthermore, very recently in the lower $N = 58$ isotone ^{92}Se , a long-lived $15.7\mu\text{s}$ isomeric state at 3072 keV was measured with the HPGe-spectrometer EURICA [35]. The isomer has been observed to decay only via a 67 keV E2 transition with a transition strength of around 1 W.u.. The authors also assigned this as a tentative (9^-) decaying into to a (7^-) state assuming single-particle character

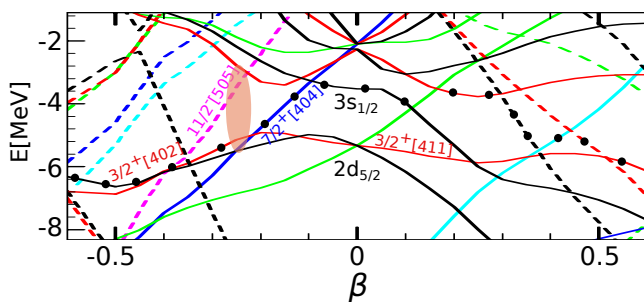


Figure 9. Partial Nilsson diagram for neutrons. The Fermi surface for $N = 58$ is denoted with black dots. Adapted from Delaroche *et al.* [31], obtained with Gogny CHFB calculations.

and identifying the two states as oblate two-quasiparticle neutron configurations $7^- = 11/2^- [505] \otimes 3/2^+ [402]$ and $9^- = 11/2^- [505] \otimes 7/2^+ [404]$ [35]. The Nilsson orbitals were determined with Gogny CHFB calculations [31]. In Fig. 9,

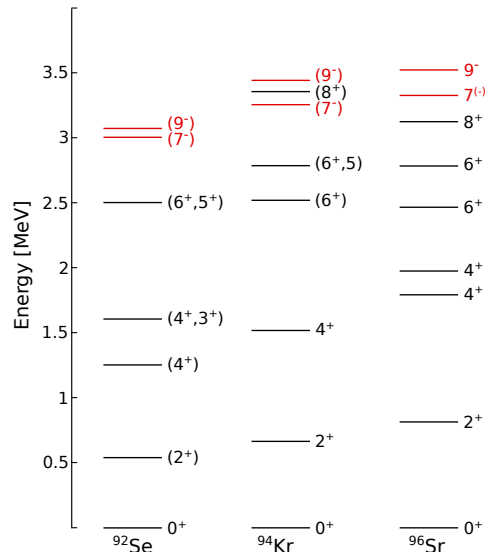


Figure 10. Comparison of partial level schemes of ^{92}Se , ^{94}Kr , and ^{96}Sr . Data from this work and Ref. [18, 33, 35, 36].

we can see the corresponding Nilsson diagram for neutrons near the Fermi level of ^{94}Kr , which is very similar to the one for ^{92}Se . At an oblate deformation of $\beta \sim -0.22$, the same two-quasiparticle states exist as in ^{92}Se (see red area in Fig. 9). Thus, the decay from (9^-) to (7^-) in ^{94}Kr can be interpreted as a transition of a neutron from the $7/2^+[404]$ to the $3/2^+[402]$ level. The orbitals involved are labeled in Fig. 9. From the microscopic point of view, the Nilsson 9^- 2qp-configuration corresponds to the shell-model $(g_{7/2}, h_{11/2})_{9^-}$ one. But, while interacting shell-model calculations are in spherical basis and deformation parameters can only be calculated in a framework of shape invariants, the Nilsson model allows for an estimation of the deformation parameter β based on the observation of unique single-particle configurations. In ^{94}Kr , the oblate deformation of the isomeric state, as deduced from the assumed Nilsson configurations in Fig. 9, is nearly the same as the one of the ground state ($\beta \sim -0.26$) as predicted by the same calculations [31]. To estimate the reduced transition strengths for the isomeric decay branches, we assume pure E1 and E2 decay branches similar to ^{96}Sr . The branching ratio of $I_{88} \approx \frac{1}{2} \cdot I_{186.8}$ is derived by analyzing the intensities of the 470.7 keV and 736.0 keV and the 834.9 keV transitions in Fig. 4. Due to the low statistics, intensity uncertainties of 50 % were assumed and propagated in the calculation. Thus, when considering a two-branch decay of the isomer with an 88 keV E1 transition and a 186.8 keV E2 transition, reduced transition strengths of $B(E1) = 4_{-2}^{+3} \cdot 10^{-6}$ W.u. and $B(E2) = 1.8_{-0.5}^{+0.5}$ W.u. are obtained.

In order to discuss aspects of the nuclear structure in the $N = 58$ isotones under the assumption that the tentative spin and parity assignments are correct, partial level schemes of

^{92}Se , ^{94}Kr , and ^{96}Sr are shown in Fig. 10. While in ^{94}Kr and ^{96}Sr the excitation energies and relative position of the 9^- and 7^- levels are relatively constant, both the excitation energies and their separation slightly decrease in ^{92}Se . In all three isotopes, the reduced E2 transition strengths of about 1 W.u. show a single-particle character for the isomeric decay. In ^{94}Kr and ^{96}Sr , a competing E1 branch is observed. This is not the case in ^{92}Se , most probably due to the higher relative position of the 8^+ state as suggested by the upsloping trend of the corresponding states in ^{96}Sr and ^{94}Kr (see Fig. 10). In Wu *et al.* [34], relative $B(E2)$ values for the internal decay of some states in ^{96}Sr were derived based on the corresponding branching ratios and normalised to one of the transitions strengths. The relative $B(E2)$ values from the yrast 6^+ to the two 4^+ states in ^{96}Sr indicated a mixing of the $4^+_{1,2}$ states [34], while in ^{92}Se the calculated relative $B(E2)$ suggest no mixing of the two 4^+ states based on the branching ratio observed by Lizarazo *et al.* [35]. Similarly, we obtained relative E1 transition strengths for the $7^- \rightarrow 6^+_{1,2}$ transitions in ^{94}Kr and ^{96}Sr . In ^{94}Kr , the $B(E1; 7^- \rightarrow 6^+_1)$ is 26(1) % of the $B(E1; 7^- \rightarrow 6^+_2)$, while in ^{96}Sr , it is only 5(1) %. This implies a much greater mixing between the two 6^+ states in ^{94}Kr compared to ^{96}Sr . In ^{92}Se , only one (6^+) state was observed though from the relatively constant excitation energies of the 6^+ states in ^{94}Kr and ^{96}Sr , one would expect a similar structure.

V. CONCLUSIONS

In conclusion, this work presents the first observation of an isomeric state in ^{94}Kr , measured using the novel hybrid spectrometer ν -Ball with its unique combination of a pulsed beam and fast-neutron induced fission of ^{238}U . Reduced E1 and E2 transition strengths for the isomer decay-branches were extracted. The isomer is interpreted as being built on a two-quasiparticle neutron state consistent with Gogny CHFB calculations, presenting a very similar isomeric spin structure as in the neighboring isotones ^{92}Se and ^{96}Sr . Additionally, the level scheme was expanded significantly, allowing to discuss nuclear structure by looking into level systematics of $N = 58$ isotones and mixing of states by comparing relative transition strengths.

ACKNOWLEDGMENTS

We thank the accelerator staff of the ALTO facility at the IPN Orsay for providing a stable beam and continuous support. This work is supported by the DFG under Grant No. BL 1513/1-1 and by the BMBF under Grants No. 05P15RDFN1, 05P19RDFN1.

-
- [1] K. Heyde and J. L. Wood, *Rev. Mod. Phys.* **83**, 1467 (2011).
 - [2] F. Schussler, J. A. Pinston, E. Monnard, A. Moussa, G. Jung, E. Koglin, B. Pfeiffer, R. V. F. Janssens, and J. van Klinken, *Nuclear Physics A* **339**, 415 (1980).
 - [3] T. A. Khan, W. D. Lauppe, K. Sistemich, H. Lawin, G. Sadler, and H. A. Selic, *Z. Phys. A* **283**, 105 (1977).
 - [4] E. Cheifetz, R. C. Jared, S. G. Thompson, and J. B. Wilhelmy, *Phys. Rev. Lett.* **25**, 38 (1970).
 - [5] F. K. Wohn, J. C. Hill, R. F. Petry, H. Dejbakhsh, Z. Berant, and R. L. Gill, *Phys. Rev. Lett.* **51**, 873 (1983).
 - [6] W. Urban *et al.*, *The European Physical Journal A - Hadrons and Nuclei* **22**, 241 (2004).
 - [7] C. Kremer *et al.*, *Phys. Rev. Lett.* **117**, 172503 (2016).
 - [8] E. Clément *et al.*, *Phys. Rev. Lett.* **116**, 022701 (2016).
 - [9] T. Togashi, Y. Tsunoda, T. Otsuka, and N. Shimizu, *Phys. Rev. Lett.* **117**, 172502 (2016).
 - [10] S. Naimi *et al.*, *Phys. Rev. Lett.* **105**, 032502 (2010).
 - [11] C. Sotty *et al.*, *Phys. Rev. Lett.* **115**, 172501 (2015).
 - [12] M. Albers *et al.*, *Phys. Rev. Lett.* **108**, 062701 (2012).
 - [13] M. Albers *et al.*, *Nuclear Physics A* **899**, 1 (2013).
 - [14] J. Dudouet *et al.*, *Phys. Rev. Lett.* **118**, 162501 (2017).
 - [15] F. Flavigny *et al.*, *Phys. Rev. Lett.* **118**, 242501 (2017).
 - [16] T. R. Rodríguez, *Phys. Rev. C* **90**, 034306 (2014).
 - [17] K. Nomura, R. Rodríguez-Guzmán, Y. M. Humadi, L. M. Robledo, and H. Abusara, *Phys. Rev. C* **96**, 034310 (2017).
 - [18] T. Rząca-Urban *et al.*, *The European Physical Journal A - Hadrons and Nuclei* **9**, 165 (2000).
 - [19] N. Jovančević *et al.*, *Acta Phys. Pol.* **B 50** (2019).
 - [20] M. Lebois, N. Jovančević, D. Thisse, R. Canavan, D. Étasse, M. Rudigier, and J. N. Wilson, *Nucl. Instr. Meth. Phys. Res. A* **960** (2020).
 - [21] T. R. England and B. F. Rider, *Los Alamos National Laboratory Report LA-UR-94-3106* (1994).
 - [22] M. Lebois, J. N. Wilson, P. Halipré, B. Leniau, I. Matea, A. Oberstedt, S. Oberstedt, and D. Verney, *Nucl. Instr. Meth. Phys. Res. A* **735**, 145 (2014).
 - [23] F. Tovesson, A. Laptev, and T. S. Hill, *Nuclear Science and Engineering* **178**, 57 (2014).
 - [24] D. Etasse *et al.*, “Fast acquisition system for nuclear research,”.
 - [25] K. Moschner, Priv. comm.; R.-B. Gerst *et al.*, in preparation.
 - [26] P. Doornenbal *et al.*, *RIKEN Accel. Prog. Rep.* **49** (2016).
 - [27] A. Sonzogni, *Nuclear Data Sheets* **103**, 1 (2004).
 - [28] S. Basu, G. Mukherjee, and A. Sonzogni, *Nuclear Data Sheets* **111**, 2555 (2010).
 - [29] G. Häfner *et al.*, *Phys. Rev. C* **100**, 024302 (2019).
 - [30] N. Saed-Samii, Computer code Transnuclear, private communication.
 - [31] J.-P. Delaroche, M. Girod, J. Libert, H. Goutte, S. Hilaire, S. Péru, N. Pillet, and G. F. Bertsch, *Phys. Rev. C* **81**, 014303 (2010).
 - [32] W. Urban *et al.*, *Nuclear Physics A* **689**, 605 (2001).
 - [33] T. Rząca-Urban, K. Sieja, W. Urban, F. Nowacki, J. L. Durell, A. G. Smith, and I. Ahmad, *Phys. Rev. C* **79**, 024319 (2009).
 - [34] C. Y. Wu, H. Hua, D. Cline, A. B. Hayes, R. Teng, R. M. Clark, P. Fallon, A. Goergen, A. O. Macchiavelli, and K. Vetter, *Phys. Rev. C* **70**, 064312 (2004).

[35] C. Lizarazo *et al.*, [Phys. Rev. Lett.](#) **124**, 222501 (2020).

[36] S. Chen *et al.*, [Phys. Rev. C](#) **95**, 041302 (2017).